Research Article | Vol. 32, No. 1 / 1 Jan 2024 / Optics Express 813
Optics EXPRESS

Lissajous singularities in Young's interference experiment

WENRUI MIAO,[1] TACO D. VISSER,[2,3,4] AND GREG GBUR[1,*]

[1] *Department of Physics and Optical Science, UNC Charlotte, Charlotte, North Carolina 28223, USA*
[2] *Department of Physics and Astronomy, Vrije Universiteit, Amsterdam 1081 HV, Netherlands*
[3] *The Institute of Optics, University of Rochester, Rochester, New York 14627, USA*
[4] *School of Physics and Electronics, Shandong Normal University, Jinan 250358, China*
[*] *gjgbur@uncc.edu*

Abstract: We explore the interference of two bichromatic vector beams in Young's interference experiment. Our analysis focuses on determining the conditions under which the superposition of such beams, emerging from the pinholes, can give rise to Lissajous-type polarization singularities on the observation screen. Two independent sufficiency conditions are derived. This analysis aids in comprehending the inherent characteristics of Lissajous singularities. To the best of our knowledge, this is the first demonstration of the singular behavior of polarization in a two-frequency field in Young's interference experiment.

1. Introduction

Singularities in wavefields have become important objects of study, both for their unusual physical properties and the use of those properties to improve optical systems. The classic singularities are optical vortices in scalar wavefields, which are lines of zero intensity in three-dimensional space around which the phase has a circulating or helical structure [1]. Beams with optical vortices have been used for a variety of applications, including free-space optical communications [2], super-resolved imaging [3], and coronagraphy [4].

In vector electromagnetic fields, optical vortices are not typically seen and instead the typical singularities encountered are polarization singularities [5], which for paraxial fields include lines of circular polarization (on which the orientation of the polarization ellipse is undefined) and surfaces of linear polarization (on which the handedness of the polarization ellipse is undefined). Polarization singularities have also been used for a number of applications, including imaging [6,7] and light-matter manipulation [8].

Both optical vortices and polarization singularities are typically studied in monochromatic fields. It is possible to generalize them further, however, and consider the types of singularities that appear in bichromatic fields where the higher frequency is a harmonic of the lower. The electric field vector then traces out a Lissajous figure instead of an ellipse; singularities of the generalized orientation of this figure are called Lissajous singularities, and were first introduced by Freund and Kessler [9,10]. These singularities, like polarization singularities and optical vortices, have potential to be used in imaging and communications, and recently a class of beams containing a single Lissajous singularity at their core was formulated [11].

Though the topology of Lissajous singularities has been well-formulated, the conditions under which Lissajous singularities can be formed, for example through interference, are still unclear. Young's interference experiment provides a unique platform for exploring a rich variety of phenomena in both classical optics and quantum optics [12]. In 2003, it was used to investigate singularities of the correlation function that appear in partially coherent light [13]. In 2009, the experiment was used to analyze the creation of polarization singularities [14]. It is natural, then, to consider Young's experiment for bichromatic fields in order to determine conditions under which Lissajous singularities can be created in interference.

#510413 https://doi.org/10.1364/OE.510413
Journal © 2024 Received 7 Nov 2023; revised 8 Dec 2023; accepted 10 Dec 2023; published 21 Dec 2023

In this study, we use Young's interference experiment to investigate the superposition of two vector beams, each possessing two frequency components, and we derive sufficiency conditions under which the Lissajous-type polarization singularities are formed on the observation screen. We give examples of the Lissajous patterns and singularities created under these conditions, and demonstrate additional cases of singularity creation.

2. Lissajous singularities

Consider a beam-like electromagnetic field traveling along the z-direction, and containing frequencies ω_a and ω_b. At position $\mathbf{r}$ and time t, its electric field can be expressed as

$$\mathbf{E}(\mathbf{r}) = \mathrm{Re}\left[\mathbf{A}(\mathbf{r})e^{-\mathrm{i}\omega_a t} + \mathbf{B}(\mathbf{r})e^{-\mathrm{i}\omega_b t}\right], \tag{1}$$

where $\mathbf{A}$ and $\mathbf{B}$ are complex vectors with x and y-components. Because these vectors are complex, a complete characterization of the electric field requires eight real numbers. In a circular polarization basis with unit vectors

$$\boldsymbol{\epsilon}_{\pm} = \frac{1}{\sqrt{2}}(\hat{\mathbf{x}} \pm \mathrm{i}\hat{\mathbf{y}}), \tag{2}$$

the electric field at each point and at each individual frequency can be written as

$$\mathbf{E} = E_l \boldsymbol{\epsilon}_+ + E_r \boldsymbol{\epsilon}_-, \tag{3}$$

with E_l and E_r the complex amplitude of the left- and right-handed component, respectively. The four Stokes parameters may be written as [15]

$$S_0 = |E_l|^2 + |E_r|^2, \tag{4}$$

$$S_1 = 2\,\mathrm{Re}[E_l^* E_r], \tag{5}$$

$$S_2 = 2\,\mathrm{Im}[E_l^* E_r], \tag{6}$$

$$S_3 = |E_l|^2 - |E_r|^2. \tag{7}$$

Using the circular basis allows us to take advantage of the simple relation between S_1 and S_2, as we will see. Because the Stokes parameters are cycle-averaged, those of the total bichromatic field are simply the sum of the parameters at each of the two frequencies, i.e.,

$$S_j = S_{j,a} + S_{j,b}, \quad j \in \{0, 1, 2, 3\}. \tag{8}$$

In analogy with polarization singularities in a monochromatic field, two types of singularities can occur in a bichromatic field [10]: singularities of handedness and singularities of orientation. Because the latter is a direct analogue of vortices, it has broad potential applications compared to singularities of handedness which are surfaces in 3-D. Thus, this paper focuses exclusively on Lissajous singularities of orientation, hereafter referred to as Lissajous singularities.

A Lissajous singularity is a polarization singularity in a bichromatic field where the total complex Stokes field S_{12} equals zero, i.e.

$$S_{12} \equiv S_1 + \mathrm{i}S_2 = 0, \tag{9}$$

which means a Lissajous singularity only appears when S_1 and S_2 both equal 0. At a singularity, the pattern's orientation angle with respect to the x-axis is undefined; this orientation angle is given by [9]

$$\tan(2\psi) = \frac{S_2}{S_1}. \tag{10}$$

In a bichromatic field, a singularity of orientation is not a simple figure like circular polarization in the monochromatic case, but is generally a Lissajous figure.

Optics EXPRESS

3. Bichromatic version of Young's experiment

Let us consider Young's setup, as sketched in Fig. 1, in which a bichromatic beam, with frequencies ω_a and ω_b and corresponding wavenumbers k_a and k_b, is normally incident on a screen $\mathcal{A}$ that contains two identical pinholes separated by a distance d. The polarization state at the two frequencies need not be equal, and may be different at each pinhole. The superposition of the fields emanating from the apertures Q_1 and Q_2 is observed at a point $P = (x, 0, \Delta z)$ on a second, parallel screen $\mathcal{B}$.

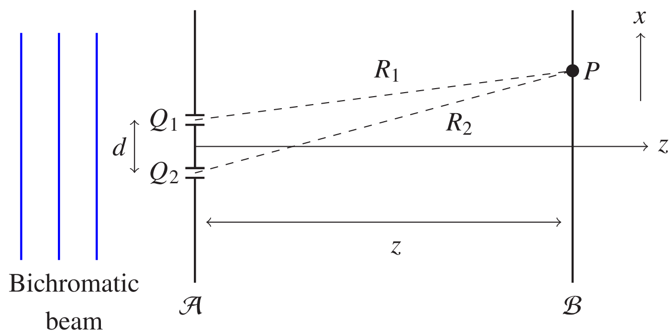

Fig. 1. Young's experiment with two frequencies. A bichromatic beam is incident on screen $\mathcal{A}$ in the plane $z = 0$, which contains two identical pinholes, Q_1 at $(d/2, 0, 0)$, and Q_2 at $(-d/2, 0, 0)$. The observation screen $\mathcal{B}$ is located in the plane $z = \Delta z$. The two distances (dashed lines) are $R_1 = Q_1P$ and $R_2 = Q_2P$.

At frequency β (with $\beta = a, b$), the transverse field at P has the form

$$\mathbf{E}_\beta(P) = A_{1,\beta} K_{1,\beta} \hat{\mathbf{e}}_{1,\beta} e^{\mathrm{i}k_\beta R_1} + A_{2,\beta} K_{2,\beta} \hat{\mathbf{e}}_{2,\beta} e^{\mathrm{i}k_\beta R_2}. \tag{11}$$

Here, $A_{i,\beta}$ represents the amplitude of the field at the βth frequency emanating from the aperture Q_i, and $\hat{\mathbf{e}}_{i,\beta}$, with $i = 1, 2$, is a unit polarization vector expressed in the circular basis, as indicated in Eq. (2), that characterizes the polarization state at the aperture Q_i. Explicitly,

$$\hat{\mathbf{e}}_{i,\beta} = p_{i,\beta} \boldsymbol{\epsilon}_+ + m_{i,\beta} \boldsymbol{\epsilon}_-, \tag{12}$$

with $|p_{i,\beta}|^2 + |m_{i,\beta}|^2 = 1$. We shall take $p_{i,\beta}$ to be complex while $m_{i,\beta}$ is assumed to be real. The propagator $K_{i,\beta}$ is given by the expression [16]

$$K_{i,\beta} = \frac{d\mathcal{A}}{\mathrm{i}\lambda_\beta R_i}, \tag{13}$$

where $d\mathcal{A}$ is the pinhole area, and $\lambda_\beta = 2\pi/k_\beta$. Under typical circumstances the two distances x and d are much smaller than the screen separation Δz. We then have to a good approximation

$$R_2 - R_1 \approx \frac{xd}{\Delta z}, \tag{14}$$

and

$$K_{1,\beta} \approx K_{2,\beta} = K_\beta. \tag{15}$$

In our derivation we make use of these two approximations, but in the simulations the exact form of the expressions will be used.

Because the propagator depends on λ_β, as seen in Eq. (13) the apertures will preferentially transmit more light of the smaller wavelength component. This will cause the smaller wavelength

Optics EXPRESS

to dominate on the observation screen and wash out any Lissajous singularities. To eliminate the difference in amplitude at the two frequencies caused by their respective propagators, we let $A_{i,\beta} = 1/K_\beta$, to obtain a normalized vector field

$$\bar{\mathbf{E}}_\beta(P) = \hat{\mathbf{e}}_{1,\beta} e^{ik_\beta R_1} + \hat{\mathbf{e}}_{2,\beta} e^{ik_\beta R_2}. \tag{16}$$

This could be done experimentally by placing appropriate spectral filters in front of the pinholes Q_i.

The resulting normalized Stokes parameters at frequency β on the observation screen are thus

$$\bar{S}_{1,\beta}(P) = 2\,\mathrm{Re}[\bar{E}^*_{l,\beta}(P)\bar{E}_{r,\beta}(P)], \tag{17}$$

$$\bar{S}_{2,\beta}(P) = 2\,\mathrm{Im}[\bar{E}^*_{l,\beta}(P)\bar{E}_{r,\beta}(P)], \tag{18}$$

where

$$\bar{E}_{l,\beta}(P) = \bar{E}_\beta(P) \cdot \boldsymbol{\epsilon}^*_+, \tag{19}$$

$$\bar{E}_{r,\beta}(P) = \bar{E}_\beta(P) \cdot \boldsymbol{\epsilon}^*_-. \tag{20}$$

For brevity we omit, from now on, the dependence on the position P. At frequency a we thus have

$$\bar{S}_{1,a} = 2\,\mathrm{Re}\left[\left(p^*_{1,a} e^{-ik_a R_1} + p^*_{2,a} e^{-ik_a R_2}\right)\left(m_{1,a} e^{ik_a R_1} + m_{2,a} e^{ik_a R_2}\right)\right], \tag{21}$$

$$\bar{S}_{2,a} = 2\,\mathrm{Im}\left[\left(p^*_{1,a} e^{-ik_a R_1} + p^*_{2,a} e^{-ik_a R_2}\right)\left(m_{1,a} e^{ik_a R_1} + m_{2,a} e^{ik_a R_2}\right)\right]. \tag{22}$$

Similar expressions are obtained for $\bar{S}_{1,b}$ and $\bar{S}_{2,b}$. Using their additive property, the Stokes parameters for the total field on the observation screen are thus

$$\bar{S}_1 = \bar{S}_{1,a} + \bar{S}_{1,b}, \tag{23}$$

$$\bar{S}_2 = \bar{S}_{2,a} + \bar{S}_{2,b}. \tag{24}$$

It is to be noted that the there are two ways to get a Lissajous singularity at a point: the Stokes vectors can be identically zero at each frequency, or the different frequency components can cancel each other out.

4. Lissajous singularities in Young's experiment

Lissajous singularities appear at points where the zeros of $\bar{S}_1$ and $\bar{S}_2$ coincide. Since these two parameters are the real and imaginary part of the same expression, it readily follows that these joint zeros imply a single condition, i.e.,

$$\begin{aligned} &p^*_{1,a}\left[m_{1,a} + m_{2,a} e^{ik_a(R_2-R_1)}\right] + p^*_{2,a}\left[m_{2,a} + m_{1,a} e^{-ik_a(R_2-R_1)}\right] \\ &+ p^*_{1,b}\left[m_{1,b} + m_{2,b} e^{ik_b(R_2-R_1)}\right] + p^*_{2,b}\left[m_{2,b} + m_{1,b} e^{-ik_b(R_2-R_1)}\right] = 0. \end{aligned} \tag{25}$$

Equation (25) can be rewritten in a compact matrix form as

$$\langle \mathbf{A}|\mathbf{M}|\mathbf{A}\rangle^\dagger = 0. \tag{26}$$

Here

$$\langle \mathbf{A}| = \left[e^{-ik_a R_1} \quad e^{-ik_a R_2} \quad e^{-ik_b R_1} \quad e^{-ik_b R_2}\right], \tag{27}$$

$|\mathbf{A}\rangle^{\dagger}$ is the adjoint of $\langle\mathbf{A}|$, and

$$\mathbf{M} = \begin{bmatrix} p_{1,a}^{*}m_{1,a} & p_{1,a}^{*}m_{2,a} & 0 & 0 \\ p_{2,a}^{*}m_{1,a} & p_{2,a}^{*}m_{2,a} & 0 & 0 \\ 0 & 0 & p_{1,b}^{*}m_{1,b} & p_{1,b}^{*}m_{2,b} \\ 0 & 0 & p_{2,b}^{*}m_{1,b} & p_{2,b}^{*}m_{2,b} \end{bmatrix}. \tag{28}$$

This matrix is non-Hermitian, which indicates the possible solutions of Eq. (26) are more complicated than those of a Hermitian matrix. A necessary condition for Eq. (26) to be satisfied is Det $\mathbf{M} = 0$, and this can be shown through direct calculation to be automatically satisfied. A more involved calculation shows that of the four eigenvalues of the matrix, two of them are zero and two are non-zero.

Because the matrix $\mathbf{M}$ is non-Hermitian, it has distinct right and left eigenvectors and these represent distinct situations when Lissajous singularities will form. Thus,

$$\langle\mathbf{A}|\mathbf{M} = \langle\mathbf{0}| \tag{29}$$

and

$$\mathbf{M}|\mathbf{A}\rangle^{\dagger} = |\mathbf{0}\rangle \tag{30}$$

are two independent sufficiency conditions to satisfy Eq. (26).

The formulation of the bichromatic interference problem in the matrix form of Eq. (26) is the most significant finding of this paper. It provides a clear method for determining the conditions under which the incident bichromatic fields on the pinholes will produce Lissajous singularities. In the next section, we will delve into the exploration of the two categories of solutions to generate Lissajous singularities on the observation plane. Since both conditions are only sufficient, it is possible to find Lissajous singularities in some situations without necessarily satisfying these sufficiency criteria. We will provide an illustrative example of such a case as well.

5. Examples and discussions

We now look at the conditions of Eqs. (29) and (30) in turn. The condition $\langle\mathbf{A}|\mathbf{M} = \langle\mathbf{0}|$ represents the pair of equations

$$p_{1,a}^{*}e^{-\mathrm{i}k_aR_1} + p_{2,a}^{*}e^{-\mathrm{i}k_aR_2} = 0, \tag{31}$$

$$p_{1,b}^{*}e^{-\mathrm{i}k_bR_1} + p_{2,b}^{*}e^{-\mathrm{i}k_bR_2} = 0. \tag{32}$$

Because R_1 and R_2 represent quasi-independent distances, and k_a and k_b are very large at optical frequencies, k_aR_1 and k_aR_2 will produce every combination of phases over the observation plane. We write k_aR_1 as ϕ_1, and k_aR_2 as ϕ_2. Since $k_b = nk_a$, with $n = 2, 3, \ldots$, Eqs. (31) and (32) can be rewritten as

$$p_{1,a}^{*}e^{-\mathrm{i}\phi_1} + p_{2,a}^{*}e^{-\mathrm{i}\phi_2} = 0, \tag{33}$$

$$p_{1,b}^{*}e^{-\mathrm{i}n\phi_1} + p_{2,b}^{*}e^{-\mathrm{i}n\phi_2} = 0. \tag{34}$$

Thus

$$\begin{aligned} p_{1,a} &= Ae^{-\mathrm{i}\phi_1}, \quad p_{2,a} = -Ae^{-\mathrm{i}\phi_2}, \\ p_{1,b} &= Be^{-\mathrm{i}n\phi_1}, \quad p_{2,b} = -Be^{-\mathrm{i}n\phi_2}, \end{aligned} \tag{35}$$

with $A, B \in \mathbb{R}$. Figures 2–4 illustrate solutions of Eq. (35) for different ratios of wavenumber and polarization states of the incident vector beams. We choose $m_{i,\beta} = (1 - |p_{i,\beta}|^2)^{1/2}$ in all these examples, with little loss of generality.

Optics EXPRESS

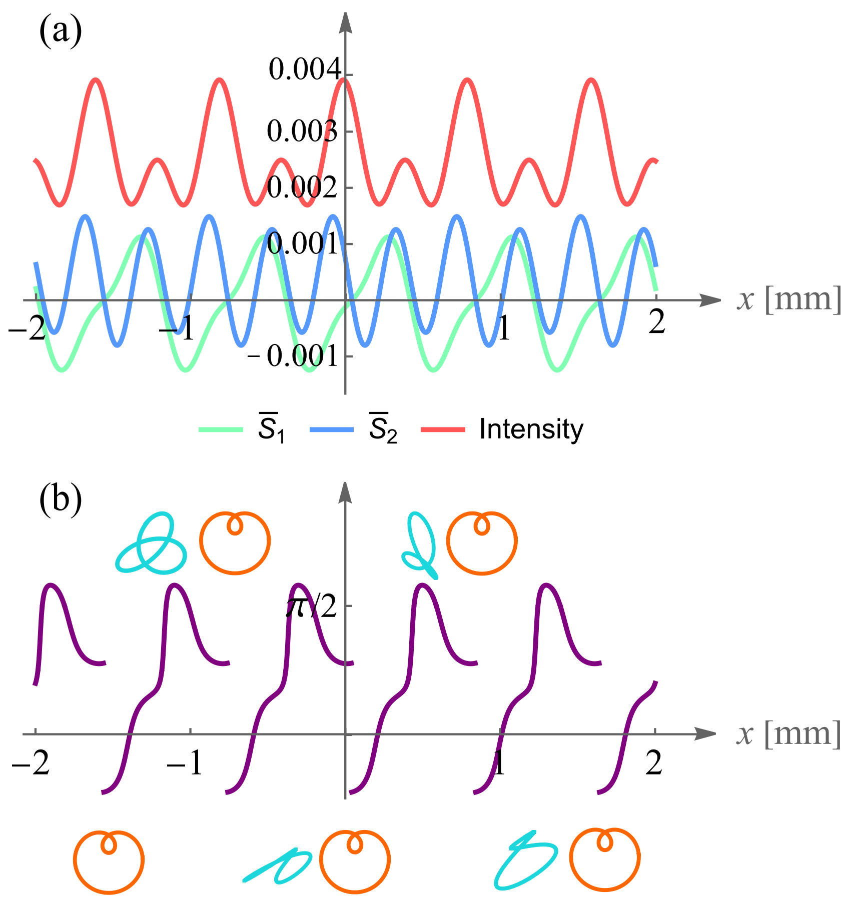

Fig. 2. (a) Intensity [a.u.] (red) and the Stokes parameters $\bar{S}_1$ (green) and $\bar{S}_2$ (blue) along the x-axis on the observation screen. (b) Lissajous singularities (orange), non-singular Lissajous patterns (cyan) and the orientation angle ψ (purple) along the x-axis on the observation screen. In this example $n = 2$, $\lambda_a = 800$ nm, $\lambda_b = 400$ nm. $p_{1,a} = (\sqrt{2}/3)\exp(\mathrm{i}3\pi/5)$, $p_{2,a} = -(\sqrt{2}/3)\exp(\mathrm{i}\pi/2)$, $p_{1,b} = (1/2)\exp(\mathrm{i}6\pi/5)$, and $p_{2,b} = (-1/2)\exp(\mathrm{i}\pi)$.

In Fig. 2(a), with $n = 2$, the intensity (solid red curve) exhibits periodic fluctuations and remains non-zero throughout. Lissajous singularities occur at the intersections of $\bar{S}_1 = 0$ and $\bar{S}_2 = 0$. In panel Fig. 2(b) it is seen that the orientation angle undergoes a $\pi/2$ jump across each singularity; an analogous $\pi/2$ change in orientation occurs when crossing a polarization singularity in a monochromatic field, regardless of whether the type of generic polarization singularity is a lemon, star or monstar [1]. Along the x-axis, a recurring array of identical "crescent" Lissajous singularities (orange curves) forms, interspersed with non-singular Lissajous patterns of diverse shapes (cyan curves).

In Fig. 3, the frequency ratio n is changed to 3, and we vary the choices of $p_{i,\beta}$. It is seen that the Lissajous singularities take on varied orientations compared to the identical orientations observed in Fig. 2. A video demonstrating the continuous evolution of Lissajous patterns along the x-axis can be found in Visualization 1.

In the previous examples, the change in polarization state was accompanied by significant changes in intensity. Figure 4 shows that this need not be the case: for an appropriate choice of parameters, Lissajous patterns can manifest along the x-axis while the overall intensity remains

Optics EXPRESS

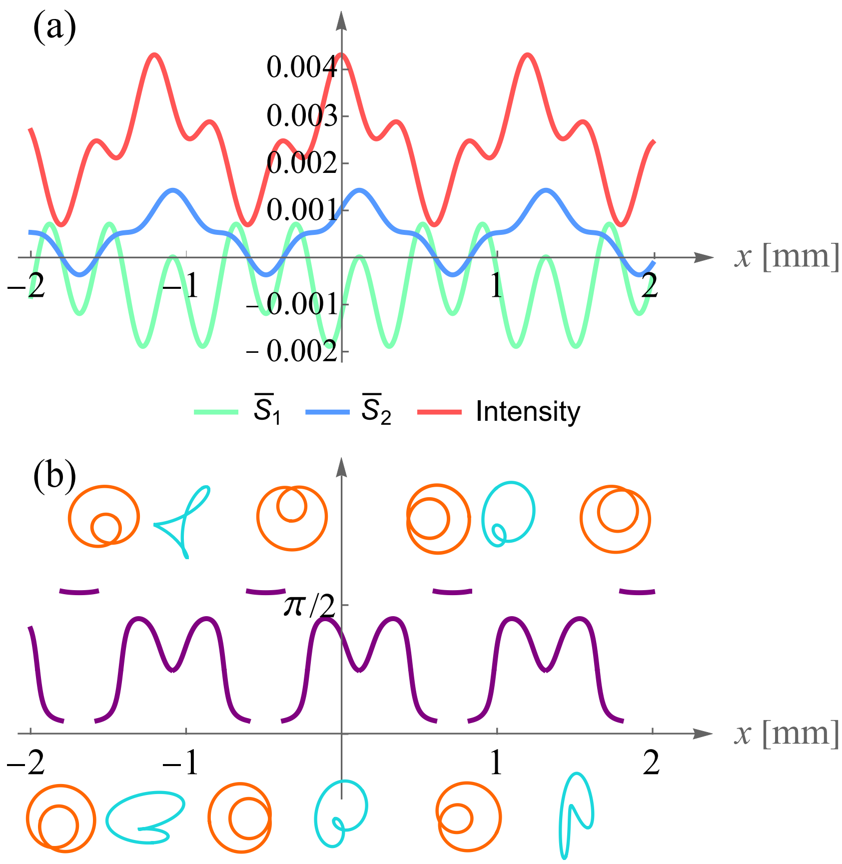

Fig. 3. (a) Intensity [a.u.] (red) and the Stokes parameters $\bar{S}_1$ (green) and $\bar{S}_2$ (blue) along the x-axis on the observation screen. (b) Lissajous singularities (orange), non-singular Lissajous patterns (cyan) and the orientation angle ψ (purple) along the x-axis on the observation screen. Here, $n = 3$, $\lambda_a = 1200$ nm, $\lambda_b = 400$ nm. $p_{1,a} = (\sqrt{2}/4)\exp(\mathrm{i}3\pi/2)$, $p_{2,a} = -(\sqrt{2}/4)\exp(\mathrm{i}\pi/8)$, $p_{1,b} = (1/2)\exp(\mathrm{i}9\pi/2)$, and $p_{2,b} = -(1/2)\exp(\mathrm{i}3\pi/8)$ (see Visualization 1).

effectively constant. In Fig. 4(a), the intensity is essentially constant over the range of interest; the intensity for each frequency is essentially constant as well. Though there is no observed pattern in intensity on the observation plane, periodic Lissajous singularities do appear at the intersections of $\bar{S}_1$ and $\bar{S}_2$ with the x-axis, as evidenced by the $\pi/2$ jumps in Fig. 4(b). In this case, Lissajous singularities are not only of crescent shape. Instead, trefoils and crescents appear alternately. This suggests a broader range of possible Lissajous singularity shapes on the observation screen. A video depicting the variation of Lissajous patterns along the x-axis in this scenario is included in Visualization 2.

We may also consider the second sufficiency condition, $\mathbf{M}|\mathbf{A}\rangle^\dagger = |\mathbf{0}\rangle$, which yields a pair of equations

$$m_{1,a}e^{\mathrm{i}k_aR_1} + m_{2,a}e^{\mathrm{i}k_aR_2} = 0, \tag{36}$$

$$m_{1,b}e^{\mathrm{i}k_bR_1} + m_{2,b}e^{\mathrm{i}k_bR_2} = 0. \tag{37}$$

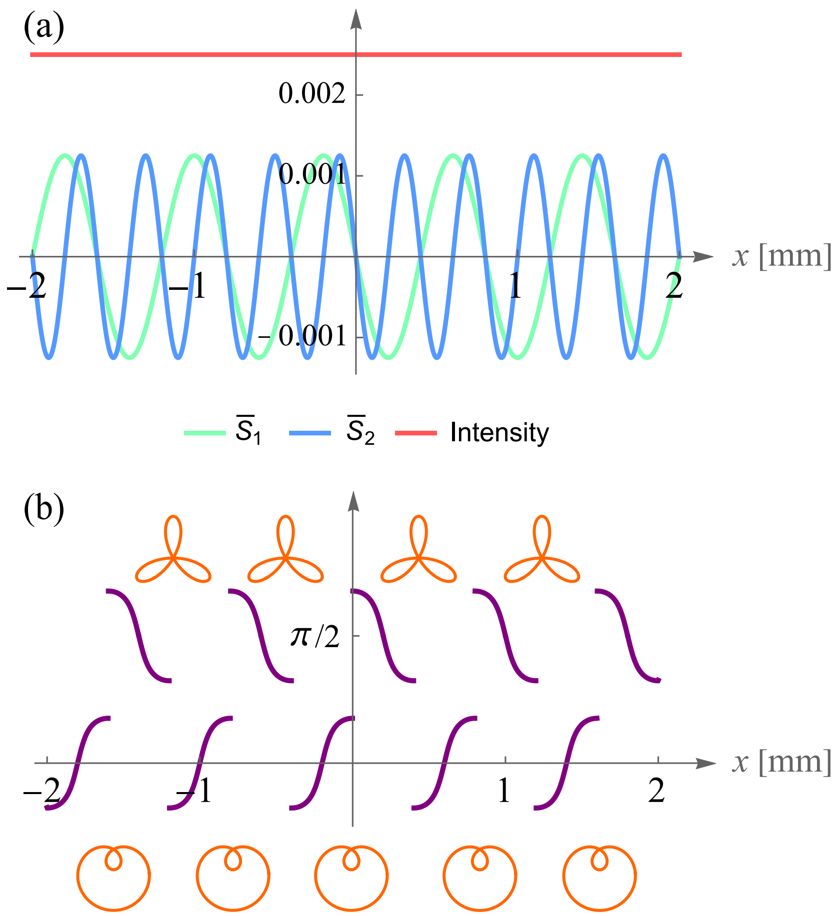

Fig. 4. (a) Intensity [a.u.] (red) and the Stokes parameters $\bar{S}_1$ (green) and $\bar{S}_2$ (blue) along the x-axis on the observation screen. (b) Lissajous singularities (orange) and the orientation angle ψ (purple) along the x-axis on the observation screen. Here, $n = 2$, $\lambda_a = 800$ nm, $\lambda_b = 400$ nm. $p_{1,a} = (\sqrt{2}/2)\exp(\mathrm{i}3\pi/2)$, $p_{2,a} = -(\sqrt{2}/2)\exp(\mathrm{i}3\pi/2)$, $p_{1,b} = (\sqrt{2}/2)\exp(\mathrm{i}3\pi)$, and $p_{2,b} = -(\sqrt{2}/2)\exp(\mathrm{i}3\pi)$ (see Visualization 2).

Using a similar notation as for the previous case, we find that

$$\begin{aligned} m_{1,a} &= Ce^{-\mathrm{i}\phi_1}, \quad m_{2,a} = -Ce^{-\mathrm{i}\phi_2}, \\ m_{1,b} &= De^{-\mathrm{i}n\phi_1}, \quad m_{2,b} = -De^{-\mathrm{i}n\phi_2}, \end{aligned} \tag{38}$$

with $C, D \in \mathbb{R}$. Because $m_{i,\beta}$ are all real as we defined in Section 3, the phases ϕ_1 and ϕ_2 can only be multiples of 2π. Thus Eqs. (38) reduce to

$$\begin{aligned} m_{1,a} &= C, \quad m_{2,a} = -C, \\ m_{1,b} &= D, \quad m_{2,b} = -D. \end{aligned} \tag{39}$$

Since $|p_{i,\beta}| = (1 - |m_{i,\beta}|^2)^{1/2}$, there is now no restriction on the phases of $p_{i,\beta}$, only on their amplitude. Thus, in the following examples these four phases are randomly chosen.

In Figs. 5 and 6 two examples are presented for which Eqs. (39) are satisfied. Irrespective of the $p_{i,\beta}$, there is always a Lissajous singularity created at $x = 0$. This is because on the z-axis,

Optics EXPRESS

$R_1 - R_2 = 0$ and hence the conditions (36) and (37) are automatically satisfied. Notice that in Fig. 5, with frequency ratio $n = 2$, again an array of identical Lissajous singularities is formed.

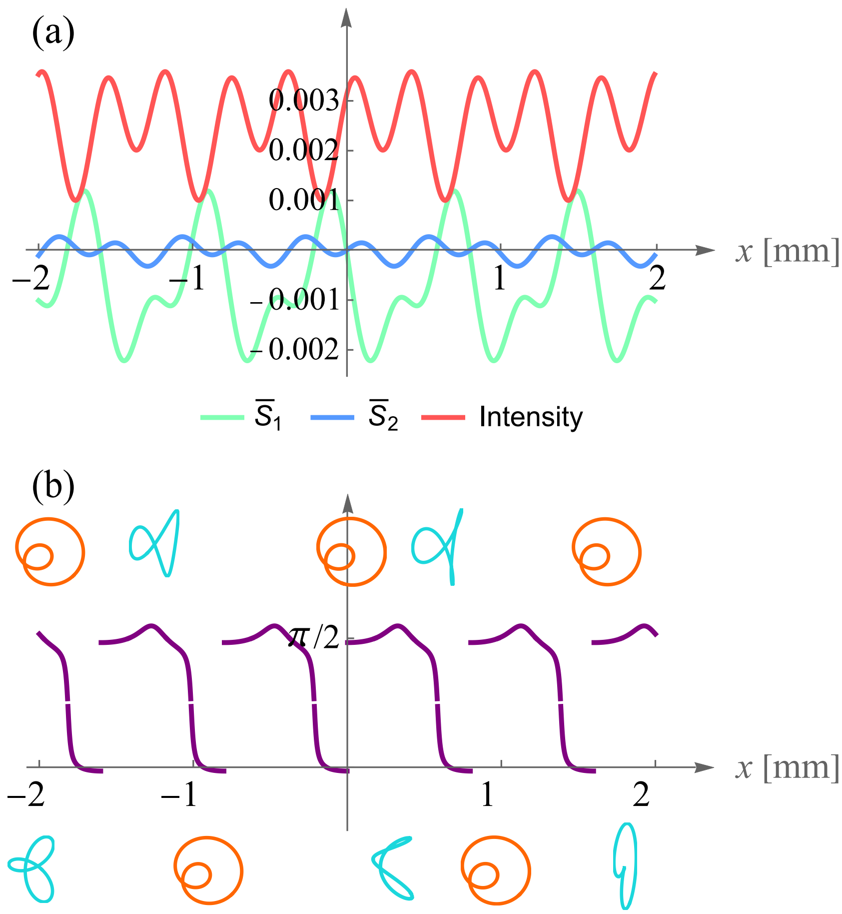

Fig. 5. (a) Intensity [a.u.] (red) and the Stokes parameters $\bar{S}_1$ (green) and $\bar{S}_2$ (blue) along the x-axis on the observation screen. (b) Lissajous singularities (orange), non-singular Lissajous patterns (cyan) and the orientation angle ψ (purple) along the x-axis on the observation screen. Here, $n = 2$, $\lambda_a = 800$ nm, $\lambda_b = 400$ nm. $m_{1,a} = \sqrt{2}/2, m_{2,a} = -\sqrt{2}/2, m_{1,b} = 1/3, m_{2,b} = -1/3, p_{1,a} = (\sqrt{2}/2)\exp(\mathrm{i}3\pi/5)$, $p_{2,a} = (\sqrt{2}/2)\exp(\mathrm{i}\pi/3)$, $p_{1,b} = (\sqrt{8}/3)\exp(\mathrm{i}2\pi/3)$, and $p_{2,b} = (\sqrt{8}/3)\exp(\mathrm{i}\pi/2)$.

In Figs. 5(b) and 6(b), the blank spots in the continuous interval of the orientation angle plots appear as $S_1 = 0$ while at those points S_2 does not equal 0. The mathematical software encounters challenges when calculating the Arctan function with an undefined value, resulting in gaps where we expect continuity.

Because Eqs. (29) and (30) are only sufficient conditions, and not necessary ones, it should be possible to find cases where Lissajous singularities appear even though neither condition is satisfied. An example of this is shown in Fig. 7.

We set $m_{i,\beta} = (1 - |p_{i,\beta}|^2)^{1/2}$, $n = 3$, $|p_{i,\beta}| = m_{i,\beta} = \sqrt{2}/2$, and the phases of $p_{i,\beta}$ are randomly chosen. Lissajous singularities appear with the same shape but different orientations. This illustrates that the two independent conditions we derived are indeed sufficient, but not necessary.

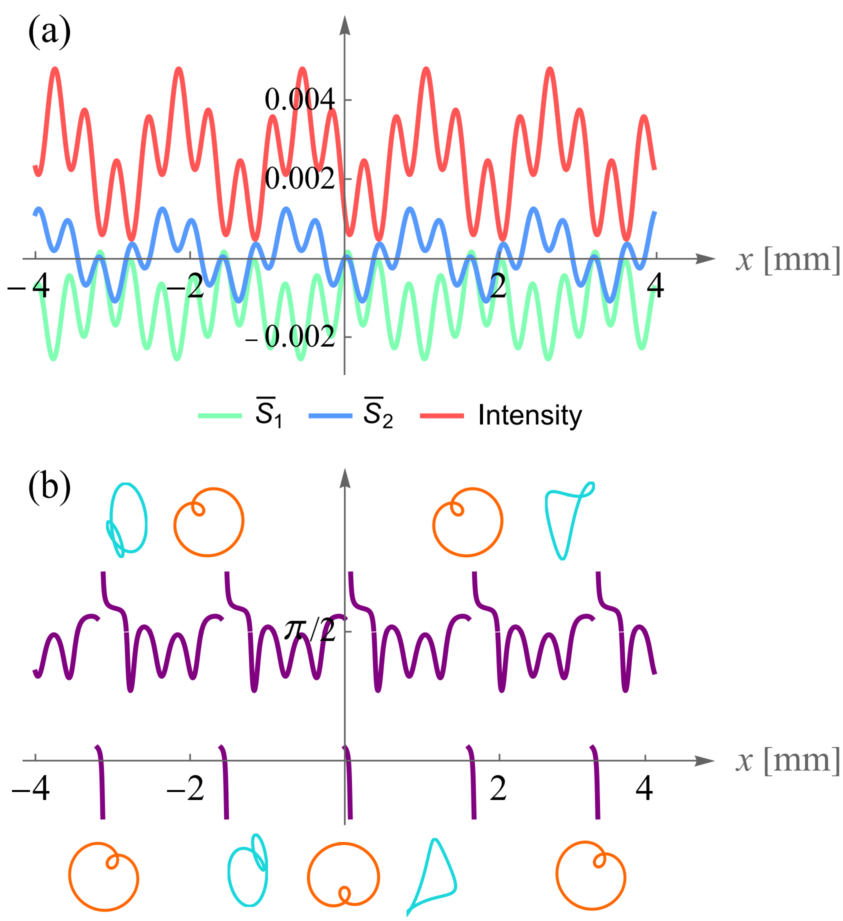

Fig. 6. (a) Intensity [a.u.] (red) and the Stokes parameters $\bar{S}_1$ (green) and $\bar{S}_2$ (blue) along the x-axis on the observation screen. (b) Lissajous singularities (orange), non-singular Lissajous patterns (cyan) and the orientation angle ψ (purple) along the x-axis on the observation screen. Here, $n = 4$, $\lambda_a = 1600$ nm, $\lambda_b = 400$ nm. $m_{1,a} = \sqrt{3}/5, m_{2,a} = -\sqrt{3}/5, m_{1,b} = 1/2, m_{2,b} = -1/2, p_{1,a} = (\sqrt{22}/5)\exp(\mathrm{i}3\pi/2)$, $p_{2,a} = (\sqrt{22}/5)\exp(\mathrm{i}\pi/8)$, $p_{1,b} = (\sqrt{3}/2)\exp(\mathrm{i}\pi)$, and $p_{2,b} = (\sqrt{3}/2)\exp(\mathrm{i}5\pi/3)$.

Optics EXPRESS

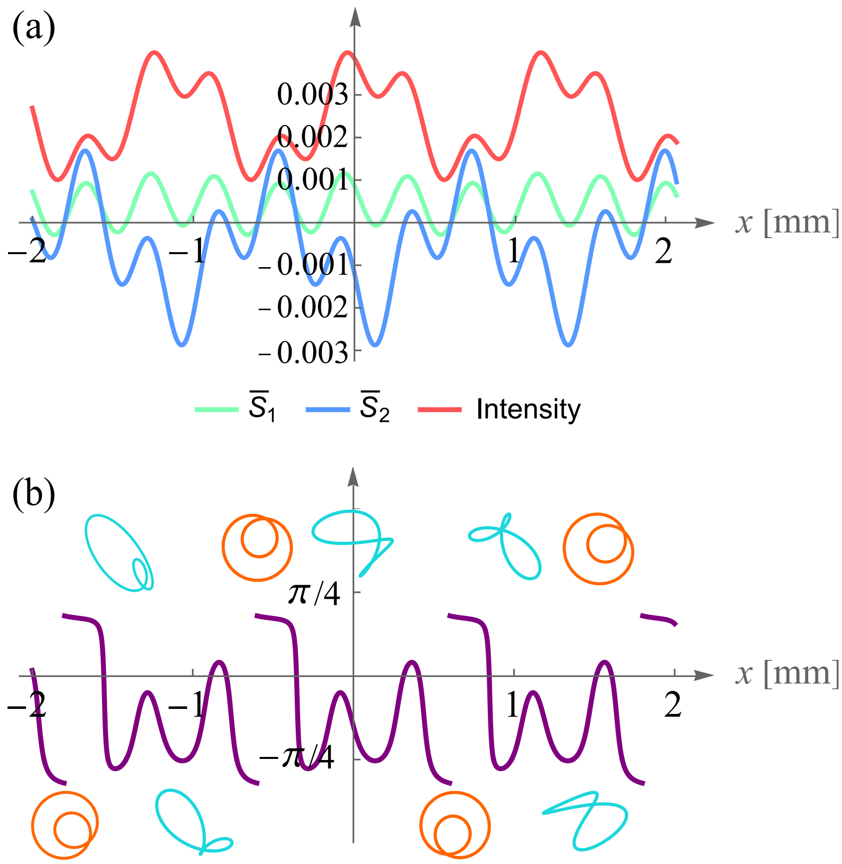

Fig. 7. (a) Intensity [a.u.] (red) and the Stokes parameters $\bar{S}_1$ (green) and $\bar{S}_2$ (blue) along the x-axis on the observation screen. (b) Lissajous singularities (orange), non-singular Lissajous patterns (cyan) and the orientation angle ψ (purple) along the x-axis on the observation screen. Here, $n = 3$, $\lambda_a = 1200$ nm, $\lambda_b = 400$ nm. $p_{1,a} = (\sqrt{2}/2)\exp(\mathrm{i}3\pi/5)$, $p_{2,a} = (\sqrt{2}/2)\exp(\mathrm{i}\pi/3)$, $p_{1,b} = (\sqrt{2}/2)\exp(\mathrm{i}4\pi/3)$, and $p_{2,b} = (\sqrt{2}/2)$.

6. Conclusions

We have examined the superposition of two bichromatic beams in Young's interference experiment, with the goal of finding conditions under which Lissajous singularities appear in interference. Two independent sufficiency conditions for the generation of Lissajous singularities were derived. Several examples, in which either of these conditions is satisfied, were presented, all showing a variety of Lissajous patterns, both singular and non-singular. Furthermore, it was demonstrated that, when neither of the two sufficiency conditions is satisfied, it is nevertheless possible to create singular polarization figures.

Though Lissajous singularities have been relatively unexplored to date, there is increasing interest in them, for example in studying unusual topological knots and Möbius strips in light waves [17]. The conditions presented in this paper should serve as a guide for future studies of such singularities.

Funding. Air Force Office of Scientific Research (FA9550-21-1-0171).

Disclosures. The authors declare no conflicts of interest.

Data availability. No data were generated or analyzed in the presented research.

Optics EXPRESS

References

1. G. Gbur, *Singular Optics* (CRC Press, Boca Raton, 2016).
2. G. Gibson, J. Courtial, M. J. Padgett, *et al.*, "Free-space information transfer using light beams carrying orbital angular momentum," Opt. Express **12**(22), 5448–5456 (2004).
3. K. Liu, Y. Cheng, Y. Gao, *et al.*, "Super-resolution radar imaging based on experimental OAM beams," Appl. Phys. Lett. **110**(16), 164102 (2017).
4. G. Foo, D. M. Palacios, and G. A. Swartzlander, "Optical vortex coronagraph," Opt. Lett. **30**(24), 3308–3310 (2005).
5. J. Hajnal, "Singularities in the transverse fields of electromagnetic waves. II. observations on the electric field," Proc. R. Soc. Lond. A **414**(1847), 447–468 (1987).
6. N. M. Garcia, I. De Erausquin, C. Edmiston, *et al.*, "Surface normal reconstruction using circularly polarized light," Opt. Express **23**(11), 14391–14406 (2015).
7. T. Ishibashi, Z. Kuang, S. Yufune, *et al.*, "Magneto-optical imaging using polarization modulation method," J. Appl. Phys. **100**(9), 093903 (2006).
8. W. Liu, W. Liu, L. Shi, *et al.*, "Topological polarization singularities in metaphotonics," Nanophotonics **10**(5), 1469–1486 (2021).
9. D. Kessler and I. Freund, "Lissajous singularities," Opt. Lett. **28**(2), 111–113 (2003).
10. I. Freund, "Bichromatic optical Lissajous fields," Opt. Commun. **226**(1-6), 351–376 (2003).
11. W. Miao and G. Gbur, "Design of Lissajous beams," Opt. Lett. **47**(2), 297–300 (2022).
12. G. Gbur and T. D. Visser, "Young's interference experiment: Past, present, and future," Prog. Opt. **67**, 275–343 (2022).
13. H. F. Schouten, G. Gbur, T. D. Visser, *et al.*, "Phase singularities of the coherence functions in Young's interference pattern," Opt. Lett. **28**(12), 968–970 (2003).
14. R. W. Schoonover and T. D. Visser, "Creating polarization singularities with an N-pinhole interferometer," Phys. Rev. A **79**(4), 043809 (2009).
15. J. D. Jackson, *Classical Electrodynamics* (Wiley, New York, 1999).
16. M. Born and E. Wolf, *Principles of Optics* (Cambridge University Press, Cambridge, 1999).
17. E. Pisanty, G. Machado, V. Vicu na-Hernández, *et al.*, "Knotting fractional-order knots with the polarization state of light," Nat. Photonics **13**(8), 569–574 (2019).